JPEDAV (2007) 28:9–22
DOI: 10.1007/s11669-006-9007-4
1547-7037 ©ASM International

First-Principles Phase Stability Calculations of Pseudobinary Alloys of $(Al,Zn)_3Ti$ with $L1_2$, $D0_{22}$, and $D0_{23}$ Structures

Gautam Ghosh, Axel van de Walle and Mark Asta

(Submitted October 24, 2006)

The thermodynamic and mechanical stability of intermetallic phases in the Al_3Ti-Zn_3Ti pseudobinary alloy system is investigated from first-principles total energy calculations through electronic density-functional theory within the generalized gradient approximation. Both supercell calculations and sublattice-cluster-expansion methods are used to demonstrate that the addition of Zn to the Al sublattice of Al_3Ti stabilizes the cubic $L1_2$ structure relative to the tetragonal $D0_{22}$ and $D0_{23}$ structures. This trend can be understood in terms of a simple rigid-band picture in which the addition of Zn modifies the effective number of valence electrons that populate bonding and anti-bonding states. The calculated zero-temperature elastic constants show that the binary end members are mechanically stable in all three ordered phases. These results point to a promising way to cost effectively achieve the stabilization of $L1_2$ precipitates in order to favor the formation of a microstructure associated with desirable mechanical properties.

Keywords cluster expansion, computational studies, crystal structure, elastic properties, electronic structure, first principles, intermetallics

1. Introduction

The trialuminide compounds with early transition metals (Sc, Ti, Zr, Hf, V, Nb, Ta) usually exhibit one or more of the three ordered structures based on the fcc lattice: cubic-$L1_2$, or tetragonal- $D0_{22}$, and $D0_{23}$. The phase stability of cubic $L1_2$-structured trialuminides is of fundamental importance for its use in at least two applications: (a) as potential high-temperature structural materials, and (b) for the design of high-temperature, creep-resistant aluminum-based alloys containing coherent precipitates. Related to (b), among binary alloy systems Al-Sc exhibits nanoscale precipitates of coherent $L1_2$-Al_3Sc as an equilibrium phase in an Al matrix.[1,2] However, the high cost of Sc limits its use in commercial alloys. Metastable Al_3Zr with the $L1_2$ structure, especially when alloyed with V, is used in commercial alloys as a grain refiner, and also to improve coarsening resistance and creep properties.[3,4] However, with prolonged aging at high temperature $L1_2$-Al_3Zr can be expected to transform to its equilibrium tetragonal structure ($D0_{23}$) with a resulting degradation of mechanical properties. Several Al-rare earth systems (RE = Er, Tm, Yb, Lu, Np) also exhibit $L1_2$-Al_3RE compounds as equilibrium phases. However, the solubility of these RE elements in Al is extremely small, so that such Al-RE alloys are not readily amenable to heat treatment. Based on these considerations, in the design of Al alloys for high-temperature applications, it is of interest to explore ternary alloy compositions which can lead to the formation of a microstructure with nanoscale precipitates of a thermodynamically stable $L1_2$ phase. Due to the extremely slow diffusion rates of Ti in Al,[5] compositions based on the binary Al-Ti system are of particular interest for such applications.

The existence of ternary $L1_2$ phases based on Al_3Ti has been reported in several Al-Ti-X (X = V, Cr, Mn, Fe, Co, Ni, Cu, Zn, Nb, Mo, Rh, Pd, Ag, Pt, and Au) systems.[6] Among these systems, the available experimental ternary phase diagrams do not show an equilibrium tie-line between Al and the $L1_2$ phase due to intervening tie-lines involving Al-Ti and Al-X intermetallics, and some ternary compounds. Even though the phase equilibria of Al-Ti-Zn has not been fully investigated, this system offers the possibility of the existence of stable tie-lines between Al and a ternary $L1_2$ phase for the following reasons: (a) there are no reported Al-Zn intermetallic phases, (b) the equilibrium $L1_2$-$TiZn_3$ phase is known to dissolve a substantial amount of

This article was presented at the Multi-Component Alloy Thermodynamics Symposium sponsored by The Alloy Phase Committee of the joint EMPMD/SMD of The Minerals, Metals, and Materials Society (TMS), held in San Antonio, TX, March 12-16, 2006, to honor the 2006 William Hume-Rothery Award recipient, Professor W. Alan Oates of the University of Salford, UK. The symposium was organized by Y. Austin Chang of the University of Wisconsin, Madison, WI, Patrice Turchi of the Lawrence Livermore National Laboratory, Livermore, CA, and Rainer Schmid-Fetzer of the Technische Universitat Clausthal, Clauthal-Zellerfeld, Germany.

Gautam Ghosh, Department of Materials Science and Engineering, Robert R. McCormick School of Engineering and Applied Science, Northwestern University, 2220 Campus Drive, Evanston, IL 60208-3108, USA; **Axel van de Walle,** Engineering and Applied Science Division, California Institute of Technology, Pasadena, CA 91125, USA; and **Mark Asta,** Department of Chemical Engineering and Materials Science, University of California at Davis, Davis, CA 95616, USA. Contact e-mail: mdasta@ucdavis.edu

Al,[7] and (c) ternary $L1_2$ phases are known to exist in the related Al-Zr-Zn and Al-Hf-Zn systems.[7] In the absence of experimental thermodynamic data for Zn-Ti and Al-Zn-Ti intermetallics, we seek to investigate the relative stability of the above-mentioned cubic and tetragonal ordered structures by first-principles methods which will ultimately facilitate the calculation of multicomponent phase diagrams within the Calphad formalism.

To investigate the relative stability of $L1_2$, $D0_{22}$, and $D0_{23}$ phases in Al-Ti-Zn alloys, we focus on the pseudobinary compositions $(Al_{1-x}Zn_x)_3Ti$. Along this line of compositions we are particularly interested in the composition dependence of the formation enthalpies as one moves from Al_3Ti, where the tetragonal structures are stable, to Zn_3Ti where the cubic $L1_2$ structure forms. In this investigation, we are thus required to compute the energies of intermetallic compounds with substitutional disorder on the Al/Zn sublattices. Within a first-principles framework we employ two complementary approaches for this purpose, namely: (a) the use of supercell (SC) geometries, and (b) the application of a sublattice-cluster-expansion (SCE) formalism[16] which has been widely used to model anion and/or cation disorder in ceramic systems.[17] As described below, the SC approach involves calculations of the energy of structures where several crystallographically equivalent sites are created by repeating the unit cell along the principle lattice directions; the energies of compounds with site-substituted species are thus calculated at discrete compositions. The SCE method involves energy calculations for several ordered superstructures representing various configurations of Al and Zn atoms on the relevant sublattices, from which values for the effective cluster interaction (ECI) parameters in a cluster expansion for the energy are extracted; with such a cluster expansion the energy can be computed as a continuous function of composition. The complementary nature of these two approaches will be illustrated below: while the SC approach allows calculations for only a relatively few discrete compositions, it can be readily used to investigate the electronic-structure features underlying the relative stabilities of the competing compounds. Such electronic-structure information is not readily available from the SCE approach, although this method allows calculations of the energy as a continuous function of composition and effects of configuration short-range order (SRO) can be estimated through Monte-Carlo simulations based on the calculated ECIs.

The next section provides further details related to the application of the complementary first-principles SC and SCE methods in their application to the study of intermetallic phase stability in Al-Ti-Zn. We discuss in particular the details related to the implementation of the SCE approach, namely the algorithms for structure and cluster selection that underly its application within the automated ATAT software.[13,14] The results of the calculations for formation energies and elastic constants are given in section 3, and the effect of Zn additions in stabilizing the cubic $L1_2$ structure is discussed within a simple band-filling picture based on the calculated electronic densities of states of the competing intermetallic phases. The results and conclusions are summarized in the final section.

2. Computational Methodology

The first-principles calculations presented here are based on electronic density-functional theory (DFT), and have been carried out using the ab-initio total-energy and molecular-dynamics program VASP (Vienna ab-initio simulation package),[8,9] employing ultrasoft pseudopotentials,[10] and an expansion of the electronic wavefunctions in plane waves with a kinetic-energy cutoff of 281 eV. All calculated results were derived employing the generalized gradient approximation (GGA) due to Perdew and Wang.[11] The remaining computational details related to the density of k-point sampling and convergence criteria for structural optimizations are the same as those described in an earlier publication.[12]

In this study, we are interested in the effect of Zn (or Al) on the relative stability of $(Al_{1-x}Zn_x)_3Ti$ phases in the $L1_2$, $D0_{22}$, and $D0_{23}$ structures. The conventional unit cells for each of these structures is illustrated in Fig. 1, where the Ti and Al/Zn sublattices are indicated by black and white circles, respectively. In the cubic $L1_2$ structure all of the Al/Zn sublattice sites are equivalent by symmetry. For the tetragonal $D0_{22}$ structure there are two symmetry-distinct Al/Zn sublattice positions, namely the 2*b* site [located in the (001) planes containing both Ti and Al/Zn atoms] and 4*d* site [located in the (001) planes containing only Al/Zn atoms]. The tetragonal $D0_{23}$ structure contains three symmetry-distinct Al/Zn sublattice sites, namely the 4*e* sites located in the (001) planes containing both Ti and Al/Zn, and two distinct sites in the pure Al/Zn (001) planes, namely 4*d* and 4*e*.

To model the compositional disorder on the Al/Zn sublattices for ternary alloy compositions, two first-principles approaches are employed. The first makes use of

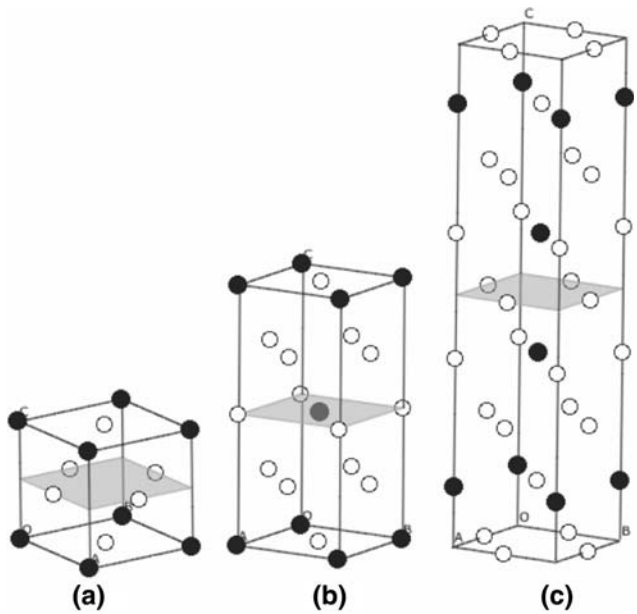

Fig. 1 Ball-and-stick model for the conventional unit cell of (a) $L1_2$, (b) $D0_{22}$, and (c) $D0_{22}$ Al_3Ti. Open and filled circles represent Al and Ti atoms, respectively. The Zn atoms are substituted in the Al sublattice only

periodic supercell (SC) structures, where several crystallographically equivalent sites are created by repeating the original unit cell along the principal lattice directions and the energy of compounds with site-substituted species are derived at discrete compositions. In the second approach ab-initio energy calculations are combined with statistical methods within the framework of the sublattice-cluster-expansion (SCE) formalism,[16] allowing predictions of thermodynamic properties as a continuous function of composition and configurational order. The details associated with each of these approaches are described in the following two subsections.

2.1 Supercell Calculations

In our application of the SC approach we have calculated the total energies of ternary alloys using supercells of 2×2×2 primitive cells for $L1_2$, and 2×2×1 for $D0_{22}$ and $D0_{23}$ structures. For the latter two structures, these supercells have dimensions of 2×2×2 fcc unit cells for $D0_{22}$ and 2×2×4 fcc unit cells for $D0_{23}$ (Fig. 1).

For the $L1_2$ structure the supercell contains 32 total sites, with 8 Ti atoms and the remaining 24 sites occupied by Al or Zn. Five compositions were considered for this structure, namely: (a) Al_3Ti, (b) $(Al_{0.667}Zn_{0.333})_3Ti$, (c) $(Al_{0.5}Zn_{0.5})_3$-Ti, (d) $(Al_{0.333}Zn_{0.667})_3Ti$, and (e) Zn_3Ti. For the ternary compositions, the atoms on the Al/Zn sublattice were arranged in an ordered manner with the minority species (for compositions (b) and (c)) having both like and unlike nearest neighbors. The $D0_{22}$ and $D0_{23}$ supercells contained 32 and 64 sites, respectively. For both phases we considered four compositions: (a) Al_3Ti, (b) $(Al_{0.667}Zn_{0.333})_3Ti$, (c) $(Al_{0.333}Zn_{0.667})_3Ti$, and (d) Zn_3Ti. For the $D0_{22}$ supercell compositions (b) and (c) were constructed by placing the minority and majority species in the 2*b*-type and 4*d* sites, respectively. In the case of the $D0_{23}$ structure, total energies for compositions (b) and (c) were calculated by substituting Zn (or Al) in all three unique sites, 4*c*, 4*d*, and 4*e*, of Al_3Ti (or Zn_3Ti); the configuration that gave the minimum energy was used for the analysis of relative phase stability. For each structure the energies were computed by first principles performing full structural optimizations with respect to volume and all (cell internal and cell external) crystallographic degrees of freedom.

2.2 Cluster Expansion and Monte-Carlo Simulations

Within the cluster-expansion (CE) formalism, the dependence of the total energy E (per unit cell) of a binary alloy on the atomic configuration σ on a given lattice is represented in the form[18]:

$$E(\sigma) = \sum_{\alpha} m_{\alpha} J_{\alpha} [\sigma_{\alpha'}] \qquad \text{(Eq 1)}$$

where the σ_i are so-called occupation variables taking the value −1 or +1, depending on which type of atom occupies site i and where $\sigma_\alpha \equiv \prod_{i \in \alpha} \sigma_i$. The sum extends over all clusters α that are symmetrically distinct while the average [...] is taken over all clusters α' that are equivalent by symmetry to α. The m_α are multiplicity coefficients equal to the number of clusters (per unit cell) equivalent to α by symmetry. The effective cluster interactions (ECI) J_α are interactions coefficients to be determined by a fit to formation energies obtained from first-principles.

Although atomic displacements do not explicitly appear in Eq 1, their effect is implicitly included in the coefficients J_α. That is, $E(\sigma)$ is actually the energy of the alloy after internal relaxations of the atomic positions and of cell parameters have taken place. In principle, the cluster expansion provides an exact representation of the configurational dependence of the energy if the sum extends over every possible cluster. In practice, the expansion is truncated to a finite number of terms that is sufficient to provide the desired accuracy. If one had knowledge of the energy of every possible configuration σ, the ECI could be exactly calculated from:

$$J_\alpha = 2^{-\#\alpha}([E(\sigma)|\sigma_\alpha = 1] - [E(\sigma)|\sigma_\alpha = -1]) \qquad \text{(Eq 2)}$$

where $\#\alpha$ is the number of sites in α and the averages [...] are taken over all configurations σ such that σ_α for the selected cluster α takes on a specific value. For some intuition, consider the special case of a Hamiltonian consisting purely of nearest neighbor interactions. Equation 2 when σ is a nearest neighbor pair would then simply reduce to half the difference between the average bond energy between like and unlike atoms (i.e., $(E_{AA} + E_{BB})/2 - E_{AB})/2$, where E_{ts} represent bond energies between atoms of type t and s). In practice, only a finite number of structural formation energies are calculated from first-principles and the ECI are not determined by Eq 2 but rather by a fit of Eq 1, truncated to a finite number of terms, to the known energies.

A sublattice-cluster-expansion (SCE) takes the same form as Eq 1 and, formally, each ECI is also exactly given by Eq 2. The efficacy of the sublattice-cluster-expansion method in understanding phase stability and phase equilibria has been demonstrated in multicomponent oxide systems.[16,17] In this study, the unit cells of $L1_2$, $D0_{22}$, and $D0_{23}$ structures are considered, allowing occupation of Zn in the Al-sublattice(s) [or Al in Zn-sublattice(s)], while, in the other sublattice, Ti acts as a spectator specie. The spectator atoms do not explicitly enter the expression of the cluster expansion because their configuration on their respective sublattice does not change. However, their presence modifies the construction of the cluster expansion in two important ways. First, the energy $E(\sigma)$ in Eq 1 and 2 includes the contribution of the spectator species so that the ECI coupling two sites also includes the indirect interaction between these sites mediated through the spectator specie. For instance, if a "larger" atom on site i pushes the spectator atom away in such a way that an atom on site j has "less room", the ECI $J_{\{i,j\}}$ coupling sites i and j will account for that energy cost, even though the spectator specie resides neither on site i nor j. The spectator atoms can also mediate interactions of a chemical nature (e.g., electronegativity differences on site i can affect the effective valence of a spectator specie, which, in turn, modifies the relative energy cost of placing different species on site j). The second important effect of the spectator species is that they lower the symmetry of the sublattice of interest, so that the ECI

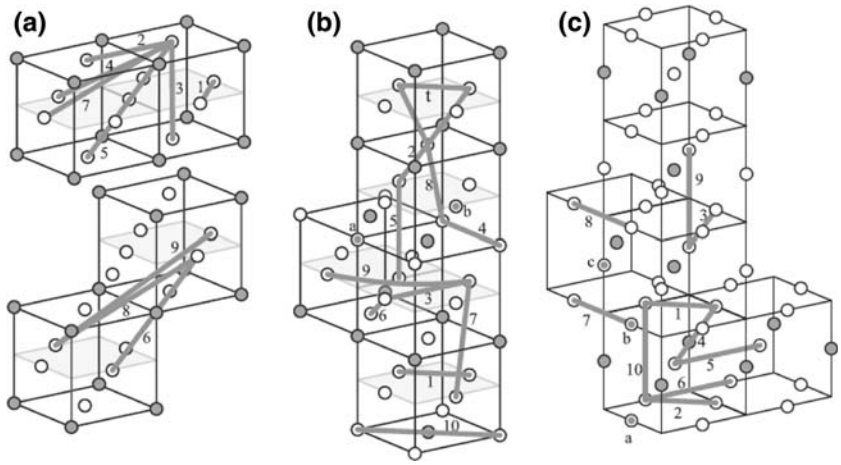

Fig. 2 Clusters included in the cluster expansions for the (a) $L1_2$, (b) $D0_{22}$, and (c) $D0_{23}$ lattices. Point clusters are indicated by a, b, ..., pair clusters by 1, 2, ... and the triplet by "t". The clusters are enumerated in the same order as in Table 4. For clarity, some of the clusters coordinates have been replaced by other, symmetrically equivalent, values

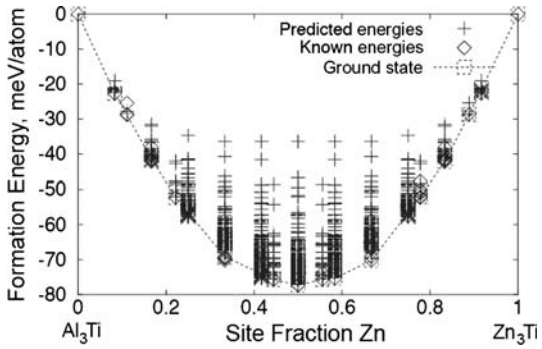

Fig. 3 Selected formation energies in the $L1_2$-$(Al,Zn)_3Ti$ system. Diamonds denote the energies (predicted from the cluster expansion) for which the ab initio energy is known. The dotted line indicates the convex hull of these energies from which the ground states (squares) can be identified. The crosses denote predicted energies for a large database of generated structures (including all structures with at most 16 atoms per unit cell) that is used to verify that all ground states have been found. The reference states used to calculate the formation energies are $L1_2$-Al_3Ti and $L1_2$-Zn_3Ti

associated with two clusters that have apparently identical geometries may still differ due to differing environments. For instance, in Fig. 2(a) and Table 4, clusters 2 and 3 for the $L1_2$ lattice have identical lengths but are considered different because cluster 2 goes through a dumbbell on spectator atoms while cluster 3 does not. Formally, cluster equivalence is determined according to the joint space group of the two sublattices.

The cluster expansion for each of the three lattices that were considered (see Fig. 1) were constructed using the Alloy Theoretic Automated Toolkit (ATAT) package.[13,14] ATAT proceeds by gradually increasing the number of clusters included in the cluster expansion and the number of structures used to fit the ECI, until the user is satisfied with the accuracy of the cluster expansion. As an example, Fig. 3 plots the formation energies of the structures used for the cluster expansion of $L1_2$ pseudobinary alloy. In this representation, the ground states in this system can be determined by identifying the points touching the convex hull. For a given set of structural energies, the optimal set of clusters is determined by minimizing the cross-validation (CV) score, defined as $\left(\sum_S (E_s - \hat{E}_{-s})^2\right)^{(1/2)}$, where E_s is the energy of structure s while $\hat{E}_{-s}$ is the energy predicted from the cluster expansion using all structures except structure s. The database of structures used in the fit of the cluster expansion is gradually enlarged by adding structures that differ as much as possible from the structures already considered in terms of the correlations σ_α.

3. Results and Discussion

In this section the results of first-principles calculations are presented related to the relative stability of the competing $L1_2$, $D0_{22}$, and $D0_{23}$ structures for the pseudobinary compositions $(Al_{1-x}Zn_x)_3Ti$. The first two subsections concern the structural, energetic, and elastic properties of the binary end-member compositions. The third subsection presents the composition dependencies of the formation energies for each of the three structures calculated by the supercell and sublattice-cluster-expansion methods described above. These results show that the $L1_2$ structure is energetically stable over a wide range of Zn compositions. In the final subsection the origin of the stabilizing effect of Zn is discussed in terms of a band-filling picture based on the calculated electronic densities of states.

3.1 Structural Properties and Phase Stability of Al_3Ti and Zn_3Ti

The total energies of Al_3Ti and Zn_3Ti having $L1_2$, $D0_{22}$, and $D0_{23}$ structures were each calculated as a function of volume, with all of the structural degrees of freedom being reoptimized at each volume. The resulting total energies were then fit to an equation of state (EOS)[19] defining the relationship between pressure (P) and volume (V) at zero

Table 1 Equilibrium cohesive properties at 0 K, as defined by the equation of state (EOS), of Al_3Ti and Zn_3Ti having one of three possible structures

Phase	Structure (space group)	EOS parameters			ΔE_f	Lattice constants	Wyckoff positions (x, y, z) (with degree(s) of freedom)
		V_0	B_0	B_0'			
Al_3Ti	$L1_2$($Pm\bar{3}m$)	15.737	10.36	4.12	−36.583	a = 0.39779	...
	$D0_{22}$ ($I4/mmm$)	15.929	10.30	4.15	−38.895	a = 0.38399	...
						c = 0.86399	...
	$D0_{23}$ ($I4/mmm$)	15.819	10.31	4.08	−39.656	a = 0.38962	Al1(4c): 0.0, $\frac{1}{2}$, 0.0
						c = 1.66713	Al2(4d): 0.0, $\frac{1}{2}$, $\frac{1}{4}$
							Al3(4e): 0.0, 0.0, 0.37519
							Ti(4e): 0.0, 0.0, 0.11875
Zn_3Ti	$L1_2$($Pm\bar{3}m$)	15.143	9.92	5.05	−19.177	a = 0.39273	...
	$D0_{22}$ ($I4/mmm$)	14.967	10.05	5.18	−9.103	a = 0.43355	...
						c = 0.61323	...
	$D0_{23}$ ($I4/mmm$)	15.131	9.71	5.67	−14.973	a = 0.40363	Ti(4e): 0.0, 0.0, 0.12540
						c = 1.48459	Zn1(4c): 0.0, $\frac{1}{2}$, 0.0
							Zn2(4d): 0.0, $\frac{1}{2}$, $\frac{1}{4}$
							Zn3(4e): 0.0, 0.0, 0.36827

Note: The units of lattice constants, V_0, B_0, and ΔE_f (with respect to fcc-Al, cph-Ti, and cph-Zn) are nm, 10^{-3} nm^3/atom, 10^{10} N/m^2 and kJ/mol, respectively. The equilibrium cell-internal degrees of freedom (Wyckoff positions) in the $D0_{23}$ structure are also provided

temperature. From the EOS, the equilibrium energy and atomic volume (V_0), as well as the bulk modulus (B_0) and its pressure derivative (B_0') were derived for all three structures. The results are given in Table 1, along with the calculated zero-temperature formation energies (ΔE_f), defined as the difference in energy between the compound and the concentration-weighted average of the energies of the constituent atomic species in the reference crystal structures given in Table 1.

Considering specifically the formation-energy values, we note that, consistent with the results of earlier calculations (discussed in detail elsewhere[12]), $D0_{23}$ is calculated to be the ground state (i.e., the lowest-energy structure at zero temperature) for the Al_3Ti composition. The crystal chemistry of Zn-Ti intermetallics has been summarized by Vassilev et al.,[20] and $L1_2$-Zn_3Ti is known to be stable at low temperature, while the tetragonal structures $D0_{22}$ and $D0_{23}$ have not been observed. Consistent with these observations, we find that $L1_2$-Zn_3Ti is the ground state structure, whereas $D0_{22}$ and $D0_{23}$ have significantly higher energies.[21] It is noteworthy that unlike the Al_3Ti system, $D0_{22}$-Zn_3Ti is far less stable compared to $D0_{23}$-Zn_3Ti.

3.2 Mechanical Stability of Al_3Ti and Zn_3Ti

In considering the relative thermodynamic stability of competing stable and metastable phases, it is important to consider whether the higher energy structures are truly metastable or whether they are mechanically or dynamically unstable in their bulk form. This issue of mechanical stability can be assessed by calculating the single-crystal elastic constants. Generally, the single-crystal elastic constants can be obtained by ab-initio electronic-structure methods by calculating the total energy as a function of appropriate lattice deformations. Depending on the crystal system and the type of imposed lattice deformation, the curvature of the total energy versus strain curves define either a particular elastic constant or a combination of elastic constants. In this study, we have calculated single-crystal elastic constants of six binary intermetallics (Al_3Ti and Zn_3Ti with $L1_2$, $D0_{22}$, and $D0_{23}$ structures) defining the end members of the pseudobinary section Al_3Ti-Zn_3Ti.

The internal energy ($E(V,\{e_i\})$) of a crystal under an infinitesimal strain e_i, referenced to the energy of the equilibrium geometry, can be written as

$$E(V,\{e_i\}) = E(V_0,0) + \frac{V_0}{2}\sum_{ij} C_{ij}e_ie_j + \ldots \quad \text{(Eq 3)}$$

where V_0 is the volume of the unstrained crystal with $E(V_0,0)$ being the corresponding energy, C_{ij}s are the single-crystal elastic constants, and the members of strain tensor $\varepsilon = \{e_i, e_j, ...\}$ are given in Voigt notation.

For the $L1_2$ structure with cubic lattice symmetry, there are three single-crystal elastic constants, C_{11}, C_{12}, and C_{44}. For the $D0_{22}$ and $D0_{23}$ phases with tetragonal lattice symmetry, there are six single-crystal elastic constants, C_{11}, C_{12}, C_{13}, C_{33}, C_{44}, and C_{66}. For both cubic and tetragonal structures, Mehl et al.[22] have summarized the appropriate lattice deformations needed to derive the C_{ij}s. Accordingly, we have calculated total energies by imposing appropriate strains up to ±3% at 0.5% intervals. The total energies versus strain were then fit with the functional forms provided by Mehl et al.[22] to extract the elastic moduli.

The calculated C_{ij}s of Al_3Ti and Zn_3Ti phases having $L1_2$, $D0_{22}$, and $D0_{23}$ structures are listed in Tables 2 and 3, respectively. For $D0_{22}$-Al_3Ti, our results are compared with available experimental data,[25] as well as previous ab-initio values for $L1_2$ and $D0_{22}$ structures calculated by DFT within the local-density approximation (LDA), using the full-

Table 2 Calculated zero-temperature single-crystal elastic constants (in 10^{10} N/m^2) of Al_3Ti in the $L1_2$, $D0_{22}$, and $D0_{23}$ structures

Al_3Ti (this study)			Al_3Ti (previous results)		
$L1_2$	$D0_{22}$	$D0_{23}$	$L1_2$, ab initio (a)	$D0_{22}$, ab initio (b)	$D0_{22}$, expt. (c)
C_{11} = 18.39	C_{11} = 19.23	C_{11} = 20.79	C_{11} = 17.70	C_{11} = 20.20	C_{11} = 21.77
C_{12} = 6.26	C_{12} = 8.28	C_{12} = 6.35	C_{12} = 7.70	C_{12} = 8.80	C_{12} = 5.77
C_{44} = 7.35	C_{13} = 4.49	C_{13} = 4.72	C_{44} = 8.50	C_{13} = 6.00	C_{13} = 4.55
	C_{33} = 21.25	C_{33} = 20.56		C_{33} = 24.30	C_3 = 21.75
	C_{44} = 9.30	C_{44} = 8.33		C_{44} = 10.0	C_{44} = 9.20
	C_{66} = 12.84	C_{66} = 10.16		C_{66} = 14.50	C_{66} = 11.65

Note: Our calculated C_{ij}s are compared with previous ab initio and experimental data
(a) FPLAPW-LDA method[23]
(b) FPLAPW-LDA method[23,24]
(c) Ref 22

Table 3 Calculated zero-temperature single-crystal elastic constants (in 10^{10} N/m^2) of Zn_3Ti in the $L1_2$, $D0_{22}$, and $D0_{23}$ structures

Zn_3Ti (this study)		
$L1_2$	$D0_{22}$	$D0_{23}$
C_{11} = 12.25	C_{11} = 16.66	C_{11} = 16.68
C_{12} = 8.79	C_{12} = 4.36	C_{12} = 5.38
C_{44} = 7.27	C_{13} = 8.69	C_{13} = 7.71
	C_{33} = 12.36	C_{33} = 12.69
	C_{44} = 5.65	C_{44} = 7.32
	C_{66} = 1.73	C_{66} = 5.46

potential linearized augmented plane-wave method.[23,24] A comparison of experimental data[25] with our calculated values for the $D0_{22}$ structure shows very good agreement for the values of C_{13}, C_{33}, C_{44}, and C_{66} in Al_3Ti. In a previous calculation,[23,24] these values were computed to be consistently higher than the present values, which is likely due to the use of the LDA approximation which is known to consistently lead to predictions of smaller equilibrium volumes and larger elastic moduli relative to the GGA used here. In both the present (GGA) and previous (LDA) calculations the value of C_{11} shows a reasonable agreement with experimental data. However, both the present and previous calculations predict C_{12} in Al_3Ti to be significantly higher than the measured value.

The requirements of mechanical stability in a cubic crystal are[26]: $C_{11}>0$, $C_{12}>0$, $(C_{11}-C_{12})>0$, $C_{44}>0$. Similarly, the requirements of mechanical stability in a tetragonal crystal are[26]: $C_{11}>0$, $C_{12}>0$, $C_{13}>0$, $C_{33}>0$, $C_{44}>0$, $C_{66}>0$, $(C_{11}-C_{12})>0$, $(C_{11}+C_{33}-2C_{13})>0$, and $(2C_{11}+C_{33}+2C_{12}-4C_{13})>0$. In Tables 2 and 3, it is important to note that even though $L1_2$-Al_3Ti, $D0_{22}$-Al_3Ti, $D0_{22}$-Zn_3Ti and $D0_{23}$-Zn_3Ti are not the lowest-energy structures, they satisfy the criteria of mechanically stability. These results imply that it is unlikely that any of these structures will be mechanically unstable at intermediate compositions along the pseudobinary section.

3.3 Effective Cluster Interaction (ECI) Parameters

The databases of structures used for the cluster expansion fit are listed in Tables 4, 5, and 6. The ECIs obtained from cluster expansions are given in Table 7. The clusters selected are schematically shown in Fig. 3. The fitted ECIs are plotted in Fig. 4 as a function of normalized interaction range. In all cases the alloy energetics are dominated by (pseudo)pair interactions, except that there is one (pseudo)-three-body interaction in $D0_{22}$. A major difference between the structures is that in $L1_2$ all ECIs are positive while in $D0_{22}$ and $D0_{23}$ the ECIs are both positive and negative. Understanding the origin of this difference is complicated by the differing crystal symmetry, number of non-equivalent Al (or Zn) sites, different arrangement of spectator specie Ti, and differences in bond lengths associated with tetragonal distortions in these different structures (see Fig. 2). It is to be noted that Fig. 4 also reports the CV score for each cluster expansion, which provides estimates of the predictive power of each cluster expansion and can be used to derive error bars on the predicted enthalpies.

In this work, we employ the cluster expansions constructed above to predict the enthalpy of formation of solid solutions in two ways. First, in the limit of a fully disordered alloy (i.e., in the Bragg-Williams approximation), the enthalpy of the alloy at composition $0<x<1$ is given by

$$H(x) = \sum_{\alpha} m_{\alpha} J_{\alpha} (2x-1)^{\#\alpha} \qquad \text{(Eq 4)}$$

where we have used the fact that $[\sigma_\alpha] = \prod_{i\in\alpha}[\sigma_i] = (2x-1)^{\#\alpha}$ if the occupation of the sites is perfectly random. A more accurate way to calculate the enthalpy of the alloy is to employ lattice-gas Monte-Carlo simulations using the cluster expansion to calculate the alloy energy (e.g., [15]). The microscopic states can then be sampled with a probability equal to the Boltzman factor, thus allowing for the possible presence of short-range order.

3.4 Phase Stability Along Al_3Ti-Zn_3Ti

Figure 5 shows a comparison of the formation energies of the $L1_2$ and $D0_{22}$ structures, as a function of Zn

Table 4 Description of the structures used in the cluster-expansion fit to calculate the formation energy of $L1_2$-$(Al_{1-x}Zn_x)_3Ti$

Structure, ID (composition)	Space group (No.)	Wyckoff positions	ΔE_f, eV/atom
0 (Al_3Ti)	$Pm\bar{3}m$(221)	Al: 3*c*, Ti: 1*a*	0.0
2 ($(Al_{0.667}Zn_{0.333})_3Ti$)	*P*4/*mmm* (123)	Al: 2*e*, Zn: 1*c*, Ti: 1*a*	−0.091933
3 ($(Al_{0.333}Zn_{0.667})_3Ti$)	*P*4/*mmm* (123)	Al: 1*c*, Zn: 2*e*, Ti: 1*a*	−0.084757
4 ($(Al_{0.833}Zn_{0.167})_3Ti$)	*P*4/*mmm* (123)	Al1: 1*c*, Al2: 4*i*, Zn: 1*d*, Ti: 1*a*, Ti: 1*b*	−0.050068
5 ($(Al_{0.833}Zn_{0.167})_3Ti$)	*Pmmm* (47)	Al1: 1*c*, Al2: 1*d*, Al3: 1*f*, Al4: 2*l*, Zn: 1*e*, Ti: 2*i*	−0.054040
7 ($(Al_{0.667}Zn_{0.333})_3Ti$)	*P*4/*mmm* (123)	Al1: 2*f*, Al2: 2*h*, Zn: 2*e*, Ti: 2*g*	−0.088519
8 ($(Al_{0.5}Zn_{0.5})_3Ti$)	*P*4/*mmm* (99)	Al1: 1*b*, Al2: 2*h*, Zn1: 1*b*, Zn2: 2*c*, Ti1: 1*a*, Ti2: 1*a*	−0.086114
10 ($(Al_{0.333}Zn_{0.667})_3Ti$)	*P*4/*mmm* (123)	Al: 2*e*, Zn1: 2*f*, Zn2: 2*h*, Ti: 2*g*	−0.071437
12 ($(Al_{0.667}Zn_{0.333})_3Ti$)	$P4_2/mmc$ (131)	Al1: 2*c*, Al2: 2*f*, Zn: 2*d*, Ti: 2*e*	−0.092750
16 ($(Al_{0.333}Zn_{0.667})_3Ti$)	$P4_2/mmc$ (131)	Al: 2*c*, Zn1: 2*d*, Zn2: 2*f*, Ti: 2*e*	−0.083724
17 ($(Al_{0.167}Zn_{0.833})_3Ti$)	*Pmnm* (47)	Al: 1*d*, Zn1: 1*c*, Zn2: 1*e*, Zn3: 1*f*, Zn4: 2*l*, Ti: 2*i*	−0.043796
18 ($(Al_{0.167}Zn_{0.833})_3Ti$)	*P*4/*mmm* (123)	Al: 1*c*, Zn1: 1*d*, Zn2: 4*i*, Ti1: 1*a*, Ti2: 1*b*	−0.042647
19 ($(Al_{0.833}Zn_{0.167})_3Ti$)	*I*4/*mmm* (139)	Al1: 2*a*, Al2: 8*f*, Zn: 2*b*, Ti: 4*c*	−0.052648
22 ($(Al_{0.5}Zn_{0.5})_3Ti$)	*Fmmm* (69)	Al1: 4*a*, Al2: 8*d*, Zn1: 4*b*, Zn2: 8*e*, Ti: 8*c*	−0.097209
24 ($(Al_{0.167}Zn_{0.833})_3Ti$)	*I*4/*mmm* (139)	Al: 2*a*, Zn1: 2*b*, Zn2: 8*f*, Ti: 4*c*	−0.047007
25 ($(Al_{0.333}Zn_{0.667})_3Ti$)	*P*4/*mmm* (123)	Al1: 1*c*, Al2: 4*k*, Zn: 1*a*, Ti: 2*f*	−0.055676
26 ($(Al_{0.667}Zn_{0.333})_3Ti$)	*Cmmm* (65)	Al1: 2*d*, Al2: 4*f*, Al3: 4*i*, Zn: 2*c*, Ti: 4*g*	−0.055190
30 ($(Al_{0.5}Zn_{0.5})_3Ti$)	*Cmmm* (65)	Al1: 2*d*, Al2: 4*f*, Zn1: 2*c*, Zn2: 4*i*, Ti: 4*g*	−0.099640
31 ($(Al_{0.333}Zn_{0.667})_3Ti$)	*Pmma* (51)	Al: 2*b*, Zn1: 2*d*, Zn2: 2*e*, Ti: 2*e*	−0.082515
33 ($(Al_{0.5}Zn_{0.5})_3Ti$)	*Cmmm* (65)	Al1: 2*c*, Al2: 4*g*, Zn1: 2*d*, Zn2: 4*f*, Ti: 4*i*	−0.100943
34 ($(Al_{0.333}Zn_{0.667})_3Ti$)	*Amm*2 (38)	Al1: 2*a*, Al2: 2*b*, Zn1: 2*a*, Zn2: 2*b*, Zn3: 4*e*, Ti: 4*d*	−0.082264
35 ($(Al_{0.167}Zn_{0.833})_3Ti$)	*Cmmm* (65)	Al: 2*c*, Zn1: 2*d*, Zn2: 4*f*, Zn3: 4*g*, Ti: 4*i*	−0.047135
36 ($(Al_{0.167}Zn_{0.833})_3Ti$)	*P*4/*mmm* (123)	Al: 1*a*, Zn1: 1*c*, Zn2: 4*k*, Ti: 2*f*	−0.045109
37 ($(Al_{0.889}Zn_{0.111})_3Ti$)	*P*4/*mmm* (123)	Al1: 2*f*, Al2: 2*h*, Al3: 4*i*, Zn: 1*d*, Ti1: 1*b*, Ti2: 2*g*	−0.033494
75 ($(Al_{0.333}Zn_{0.667})_3Ti$)	*P*4/*mmm* (123)	Al1: 1*d*, Al2: 2*f*, Zn1: 2*h*, Zn2: 4*i*, Ti1: 1*b*, Ti2: 2*g*	−0.076372
78 ($(Al_{0.667}Zn_{0.333})_3Ti$)	*Pmmm* (47)	Al1: 1*b*, Al2: 1*h*, Al3: 2*n*, Al4: 2*p*, Zn1: 1*c*, Zn2: 2*o*, Ti1: 1*e*, Ti2: 2*m*	−0.091997
101 ($(Al_{0.222}Zn_{0.778})_3Ti$)	*Pmmm* (47)	Al1: 1*c*, Al2: 1*h*, Zn1: 1*b*, Zn2: 2*n*, Zn3: 2*o*, Zn4: 2*p*, Ti1: 1*e*, Ti2: 2*m*	−0.058077
105 ($(Al_{0.889}Zn_{0.111})_3Ti$)	*C*2/*m* (12)	Al1: 4*f*, Al2: 4*i*, Al3: 8*j*, Zn: 2*c*, Ti1: 2*d*, Ti2: 4*i*	−0.035872
132 ($(Al_{0.222}Zn_{0.778})_3Ti$)	*C*2 (5)	Al: 4*c*, Zn1: 2*b*, Zn2: 4*c*, Zn3: 4*c*, Zn4: 4*c*, Ti1: 2*b*, Ti2: 4*c*	−0.059771
133 ($(Al_{0.333}Zn_{0.667})_3Ti$)	$P\bar{3}m1$(164)	Al: 3*f*, Zn: 6*i*, Ti1: 1*b*, Ti2: 2*d*	−0.072397
135 ($(Al_{0.222}Zn_{0.778})_3Ti$)	*C*2/*m* (12)	Al: 4*i*, Zn1: 2*c*, Zn2: 4*f*, Zn3: 8*j*, Ti1: 2*d*, Ti2: 4*i*	−0.060536
136 ($(Al_{0.111}Zn_{0.889})_3Ti$)	*C*2/*m* (12)	Al: 2*d*, Zn1: 4*f*, Zn2: 4*i*, Zn3: 8*j*, Ti1: 2*c*, Ti2: 4*i*	−0.031512
137 ($(Al_{0.889}Zn_{0.111})_3Ti$)	*Cmmm* (65)	Al1: 4*f*, Al2: 4*g*, Al3: 8*q*, Zn: 2*a*, Ti1: 2*b*, Ti2: 4*g*	−0.037603
144 ($(Al_{0.778}Zn_{0.222})_3Ti$)	*P*2/*m* (10)	Al1: 1*b*, Al2: 2*m*, Al3: 2*n*, Al4: 2*n*, Zn1: 1*d*, Zn2: 1*f*, Ti1: 1*g*, Ti2: 2*m*	−0.069273
169 ($(Al_{0.556}Zn_{0.444})_3Ti$)	*P*2/*m* (10)	Al1: 1*b*, Al2: 1*d*, Al3: 1*f*, Al4: 2*n*, Zn1: 2*m*, Zn2: 2*n*, Ti1: 1*g*, Ti2: 2*m*	−0.099920
172 ($(Al_{0.833}Zn_{0.167})_3Ti$)	*P*2/*m* (10)	Al1: 1*f*, Al2: 2*n*, Zn1: 1*b*, Zn2: 1*d*, Zn3: 2*m*, Zn4: 2*n*, Ti1: 1*g*, Ti2: 2*m*	−0.083326
180 ($(Al_{0.444}Zn_{0.556})_3Ti$)	*Amm*2 (38)	Al1: 4*d*, Al2: 4*e*, Zn1: 2*a*, Zn2: 4*e*, Zn3: 4*e*, Ti1: 2*a*, Ti2: 4*d*	−0.096553
182 ($(Al_{0.222}Zn_{0.778})_3Ti$)	*Amm*2 (38)	Al: 4*d*, Zn2: 4*d*, Zn3: 4*e*, Zn4: 4*e*, Ti1: 2*a*, Ti2: 4*d*	−0.059509
187 ($(Al_{0.444}Zn_{0.556})_3Ti$)	*P*2/*m* (10)	Al1: 2*m*, Al2: 2*n*, Zn1: 1*b*, Zn2: 1*d*, Zn3: 1*f*, Zn4: 2*n*, Ti1: 1*g*, Ti2: 2*m*	−0.097267
200 ($(Al_{0.222}Zn_{0.778})_3Ti$)	*Cmmm* (65)	Al: 4*f*, Zn1: 2*a*, Zn2: 4*g*, Zn3: 8*q*, Ti1: 2*b*, Ti2: 4*g*	−0.054539
201 ($(Al_{0.222}Zn_{0.778})_3Ti$)	*P*2/*m* (10)	Al1: 1*b*, Al2: 1*d*, Zn1: 1*f*, Zn2: 2*m*, Zn3: 2*n*, Zn4: 2*n*, Ti1: 1*g*, Ti2: 2*m*	−0.060235
430 ($(Al_{0.778}Zn_{0.222})_3Ti$)	*Pmmm* (47)	Al1: 1*d*, Al2: 1*e*, Al3: 2*j*, Al4: 2*l*, Al5: 2*l*, Zn1: 1*c*, Zn2: 1*f*, Zn3: 2*k*, Ti1: 2*i*, Ti2: 2*i*	−0.091826
1091 ($(Al_{0.833}Zn_{0.167})_3Ti$)	*Cmca* (64)	Al1: 4*a*, Al2: 8*e*, Al3: 8*f*, Zn: 4*b*, Ti: 8*e*	−0.054075
1297 ($(Al_{0.167}Zn_{0.833})_3Ti$)	*Cmca* (64)	Al: 4*b*, Zn1: 4*a*, Zn2: 8*e*, Zn3: 8*f*, Ti: 8*e*	−0.046601
1635 ($(Al_{0.917}Zn_{0.083})_3Ti$)	*I*4/*mmm* (139)	Al1: 2*b*, Al2: 4*c*, Al3: 16*n*, Zn: 2*a*, Ti: 8*h*	−0.028708
1689 ($(Al_{0.417}Zn_{0.167})_3Ti$)	*Immm* (71)	Al1: 2*d*, Al2: 8*n*, Zn1: 2*a*, Zn2: 2*b*, Zn3: 2*c*, Zn4: 8*l*, Ti: 8*m*	−0.095250
1705 ($(Al_{0.083}Zn_{0.917})_3Ti$)	*I*4/*mmm* (139)	Al: 2*b*, Zn1: 2*a*, Zn2: 4*c*, Zn3: 16*n*, Ti: 8*h*	−0.023288
2078 ($(Al_{0.25}Zn_{0.75})_3Ti$)	*Cmmm* (65)	Al: 2*a*, Al2: 4*h*, Zn1: 2*b*, Zn2: 4*f*, Zn3: 4*g*, Zn4: 4*h*, Zn5: 4*j*, Ti: 8*p*	−0.066126
1 (Zn_3Ti)	$Pm\bar{3}m$(221)	Zn: 3*c*, Ti: 1*a*	0.0

Note: Here, the formation energies (ΔE_f) are relative to $L1_2$-Al_3Ti and $L1_2$-Zn_3Ti.

Table 5 Description of structures used in cluster-expansion fits to calculate the formation energy of $D0_{22}$-$(Al_{1-x}Zn_x)_3Ti$

Structure, ID (composition)	Space group (#)	Wyckoff positions	ΔE_f (eV/atom)
0 (Al_3Ti)	*I*4/*mmm* (139)	Al1: 2*b*, Al2: 4*d*, Ti: 2*a*	0.0
2 ($(Al_{0.833}Zn_{0.167})_3Ti$)	*P*4/*mmm* (123)	Al1: 1*c*, Al2: 4*i*, Zn: 1*b*, Ti1: 1*a*, Ti2: 1*d*	0.020019
3 ($(Al_{0.667}Zn_{0.333})_3Ti$)	*I*4/*mmm* (139)	Al: 4*d*, Zn: 2*b*, Ti: 2*a*	0.048280
4 ($(Al_{0.833}Zn_{0.167})_3Ti$)	*P*4/*mmm* (123)	Al1: 1*a*, Al2: 1*b*, Al3: 1*c*, Al4: 2*g*, Zn: 1*d*, Ti: 2*g*	0.005135
6 ($(Al_{0.5}Zn_{0.5})_3Ti$)	$P\bar{4}m2$(115)	Al1: 1*a*, Al2: 1*b*, Al3: 1*d*, Zn1: 1*c*, Zn2: 2*g*, Ti: 2*g*	0.062123
7 ($(Al_{0.667}Zn_{0.333})_3Ti$)	*P*4/*nmm* (129)	Al1: 2*a*, Al2: 2*c*, Zn: 2*b*, Ti: 2*c*	0.006048
9 ($(Al_{0.333}Zn_{0.667})_3Ti$)	*P*4/*nmm* (129)	Al: 2*a*, Zn1: 2*b*, Zn2: 2*c*, Ti: 2*c*	0.033561
10 ($(Al_{0.667}Zn_{0.333})_3Ti$)	$I\bar{4}m2$(119)	Al1: 2*b*, Al2: 2*c*, Zn: 2*d*, Ti: 2*a*	0.016087
11 ($(Al_{0.5}Zn_{0.5})_3Ti$)	$P\bar{4}m2$(115)	Al1: 1*b*,Al2: 2*g*, Zn1: 1*d*, Zn2: 2*g*, Ti1: 1*a*, Ti2: 1*c*	0.047775
12 ($(Al_{0.333}Zn_{0.667})_3Ti$)	$I\bar{4}m2$(119)	Al: 2*d*, Zn1: 2*b*, Zn2: 2*c*, Ti: 2*a*	0.073735
13 ($(Al_{0.667}Zn_{0.333})_3Ti$)	$P4_2/mmc$ (131)	Al1: 2*c*, Al2: 2*f*, Zn: 2*e*, Ti: 2*d*	0.016289
14 ($(Al_{0.5}Zn_{0.5})_3Ti$)	*Pmmm* (47)	Al1: 1*g*, Al2: 2*j*, Zn1: 1*b*, Zn2: 2*k*, Ti1: 1*a*, Ti2: 1*h*	0.047411
15 ($(Al_{0.667}Zn_{0.333})_3Ti$)	$P4_2/mmc$ (131)	Al1: 2*e*, Al2: 2*d*, Zn: 2*f*, Ti: 2*c*	0.071275
16 ($(Al_{0.5}Zn_{0.5})_3Ti$)	$P\bar{4}m2$(115)	Al1: 1*c*, Al2: 2*g*, Zn1: 1*a*, Zn2: 1*b*, Zn3: 1*d*, Ti: 2*g*	0.013879
17 ($(Al_{0.333}Zn_{0.667})_3Ti$)	*Pmm*2 (25)	Al1: 1*c*, Al2: 1*d*, Zn1: 1*a*, Zn2: 1*b*, Zn3: 1*b*, Zn4: 1*c* Ti1: 1*a*, Ti2: 1*d*	0.030307
19 ($(Al_{0.333}Zn_{0.667})_3Ti$)	*I*4/*mmm* (139)	Al: 2*b*, Zn: 4*d*, Ti: 2*a*	0.005666
373 ($(Al_{0.167}Zn_{0.833})_3Ti$)	*Pmnm* (59)	Al: 2*b*, Zn1: 2*b*, Zn2: 4*f*, Zn3: 4*f*, Ti1: 2*a*, Ti2: 2*a*	0.002721
376 ($(Al_{0.833}Zn_{0.167})_3Ti$)	$I4_1/amd$ (141)	Al1: 4*b*, Al2: 16*f*, Zn: 4*a*, Ti: 8*e*	0.015260
396 ($(Al_{0.667}Zn_{0.333})_3Ti$)	*Imma* (74)	Al1: 4*b*, Al2: 4*e*, Al3: 8*g*, Zn: 8*g*, Ti1: 4*a*, Ti2: 4*e*	0.012183
432 ($(Al_{0.583}Zn_{0.417})_3Ti$)	*C*2 (5)	Al1: 2*a*, Al2: 2*a*, Al3: 2*b*, Al4: 4*c*, Al5: 4*c*, Zn1: 2*b*, Zn2: 4*c* Zn3: 4*c*, Ti1: 4*c*, Ti2: 4*c*	0.034503
898 ($(Al_{0.833}Zn_{0.167})_3Ti$)	*C*2/*m* (12)	Al: 2*b*, Zn1: 2*c*, Zn2: 4*i*, Zn3: 4*i*, Ti: 4*i*	0.00000
1011 ($(Al_{0.833}Zn_{0.167})_3Ti$)	*P*4/*mmm* (129)	Al1: 2*b*, Al2: 2*c*, Al3: 2*c*, Al4: 4*f*, Zn: 2*a*, Ti1: 2*c*, Ti2: 2*c*	0.003981
1121 ($(Al_{0.667}Zn_{0.333})_3Ti$)	*P*4/*mmm* (123)	Al1: 1*a*, Al2: 1*b*, Al3: 2*h*, Al4: 4*i*, Zn: 4*i*, Ti1: 1*c*, Ti2: 1*d* Ti3: 2*g*	0.007385
1300 ($(Al_{0.5}Zn_{0.5})_3Ti$)	*P*4/*nmm* (129)	Al1: 2*a*, Al2: 2*c*, Al3: 2*c*, Zn1: 2*b*, Zn2: 4*f*, Ti1: 2*c*, Ti2: 2*c*	0.008472

Note: Here, the formation energies (ΔE_f) are relative to $D0_{22}$-Al_3Ti and $D0_{22}$-Zn_3Ti.

concentration along the pseudobinary section $(Al_{1-x}Zn_x)_3Ti$, calculated by cluster expansion, using the random occupation approximation, and Monte-Carlo simulation to include the effect of short-range ordering. In Fig. 5(a) and (b), the solid line corresponds to calculated formation energy due to random mixing of Al and Zn in the 3*c* site of the $L1_2$ structure and in the 2*b* and 4*d* sites of the $D0_{22}$ structure, while triangles and + symbols represent the calculated formation energy accounting for short range ordering in Monte-Carlo simulations at 2000 and 1000 K, respectively. As the temperature is lowered, strong ordering or clustering tendencies would be manifested in a pronounced temperature dependence of the calculated formation energies, which is seen to be absent in the Monte-Carlo results.

Therefore, our Monte-Carlo simulations show that the thermodynamic properties of the alloy can reliably be obtained within the approximation that the alloy is fully disordered (in the Al/Zn sublattice) in all three structures. Within this approximation, the free energy of the alloy simply takes the form of a ideal solution entropy term and an enthalpy term. Since the ideal solution entropies for all three types of lattices are the same (as they have the same ratio of the number of Al, Zn sites to the total number of sites), any differences in the free energies between the different types of solid solutions must arise from differences in the enthalpic terms. In other words, these simulations show that the thermodynamic properties of the alloy can reliably be obtained within the approximation that the alloy is fully disordered. Hence, the formation enthalpy of the fully disordered state provides all information needed to assess the relative stability of disordered solid solutions based on the $L1_2$, $D0_{22}$, and $D0_{23}$ superstructures.

Figure 6 represents the central result of the current study. It plots the calculated formation energies of the $L1_2$-, $D0_{22}$-, and $D0_{23}$ structures as a function of Zn concentration along the pseudobinary section $(Al_{1-x}Zn_x)_3Ti$. As discussed above, the $L1_2$ structure has the lowest energy for the composition Zn_3Ti, while it is significantly higher in energy than the tetragonal $D0_{22}$, and $D0_{23}$ structures for Al_3Ti. For the ternary compositions, the filled circles and solid lines represent the results of the supercell and sublattice-cluster-expansion calculations, respectively, which are seen to be in good overall agreement. The most striking feature of the results concerns the effect of Zn additions starting from the Al_3Ti composition. While such additions increase the energy of both tetragonal structures, Zn is seen to lower

Table 6 Description of structures used in cluster-expansion fits to calculate the formation energy of $D0_{23}$-$(Al_{1-x}Zn_x)_3Ti$

Structure, ID (composition)	Space group (#)	Wyckoff positions	ΔE_f (eV/atom)
0 (Al_3Ti)	*I*4/*mmm* (139)	Al1: 4*c*, Al2: 4*d*, Al3: 4*e*, Ti: 4*e*	0.0
2 ($(Al_{0.971}Zn_{0.083})_3Ti$)	*Pmmm* (47)	Al1: 1*d*, Al2: 1*e*, Al3: 1*f*, Al4: 2*j*, Al5: 2*k*, Al6: 2*l*, Al7: 2*i* Zn: 1*c*, Ti1: 2*l*, Ti2: 2*i*	−0.021102
4 ($(Al_{0.833}Zn_{0.167})_3Ti$)	*Immm* (71)	Al1: 2*d*, Al2: 4*e*, Al3: 4*f*, Zn: 2*c*, Ti: 4*e*	−0.038995
5 ($(Al_{0.833}Zn_{0.167})_3Ti$)	$P4_2/mmc$ (131)	Al1: 2*a*, Al2: 2*e*, Al3: 2*f*, Al4: 4*i*,Zn: 2*b*, Ti: 4*i*	−0.038480
6 ($(Al_{0.75}Zn_{0.25})_3Ti$)	$P4_2/mmc$ (131)	Al1: 1*d*, Al2: 2*i*, Al3: 2*j*, Al4: 2*k*, Al5: 2*l* Zn1: 1*c*, Zn2: 1*e*, Zn3: 1*f*, Ti1: 2*i*, Ti2: 2*l*	−0.042754
7 ($(Al_{0.667}Zn_{0.333})_3Ti$)	*I*4/*mmm* (139)	Al1: 4*d*, Al2: 4*e*, Zn: 4*c*, Ti: 4*e*	−0.046592
8 ($(Al_{0.971}Zn_{0.083})_3Ti$)	$P\bar{4}m2$(115)	Al1: 1*a*, Al2: 1*b*, Al3: 1*c*, Al4: 2*e*, Al5: 2*f*, Al6: 2*g*, Al7: 2*g* Zn: 1*d*, Ti1: 2*g*, Ti2: 2*g*	−0.005213
17 ($(Al_{0.583}Zn_{0.417})_3Ti$)	$P\bar{4}m2$(115)	Al1: 1*a*, Al2: 1*b*, Al3: 1*c*, Al4: 2*g*, Al5: 2*g* Zn1: 1*d*, Zn2: 2*e*, Zn3: 2*f*, Ti1: 2*g*, Ti2: 2*g*	−0.038136
52 ($(Al_{0.667}Zn_{0.333})_3Ti$)	*I*4/*mmm* (139)	Al1: 4*c*, Al2: 4*e*, Zn: 4*d*, Ti: 4*e*	−0.017421
58 ($(Al_{0.333}Zn_{0.667})_3Ti$)	*I*4/*mmm* (139)	Al: 4*e*, Zn1: 4*c*, Zn2: 4*d*, Ti: 4*e*	−0.032755
112 ($(Al_{0.667}Zn_{0.333})_3Ti$)	*Pmm*2 (25)	Al1: 1*a*, Al2: 1*b*, Al3: 1*b*, Al4: 1*b*, Al5: 1*c*, Al6: 1*c*, Al7: 1*d* Al8: 1*d*, Zn1: 1*a*, Zn2: 1*b*, Zn3: 1*c*, Zn4: 1*c*, Ti1: 1*a*, Ti2: 1*a* Ti3: 1*d*, Ti4: 1*d*	−0.018288
239 ($(Al_{0.417}Zn_{0.593})_3Ti$)	*Pmm*2 (25)	Al1: 1*b*, Al2: 1*b*, Al3: 1*c*, Al4: 1*d*, Al5: 1*d* Zn1: 1*a*, Zn2: 1*a*, Zn3: 1*b*, Zn4: 1*b*, Zn5: 1*c*, Zn6: 1*c*, Zn7: 1*c* Ti1: 1*a*, Ti2: 1*a*, Ti3: 1*d*, Ti4: 1*d*	−0.009778
275 ($(Al_{0.5}Zn_{0.5})_3Ti$)	*P*4/*mmm* (123)	Al1: 2*e*, Al2: 2*h*, Zn1: 2*f*, Zn2: 2*g*, Zn3: 4*i*, Ti1: 2*g*, Ti2: 2*h*	−0.025242
279 ($(Al_{0.25}Zn_{0.75})_3Ti$)	*Pmmm* (47)	Al1: 1*d*, Al2: 2*l*, Zn1: 1*c*, Zn2: 1*e*, Zn3: 1*f*, Zn4: 2*i*, Zn5: 2*j* Zn6: 2*k*, Ti1: 2*i*, Ti2: 2*l*	−0.031401
283 ($(Al_{0.833}Zn_{0.167})_3Ti$)	*I*4*mm* (107)	Al1: 2*a*, Al2: 4*b*, Al3: 4*b*, Zn: 2*a*, Ti1: 2*a*, Ti2: 2*a*	−0.014853
355 ($(Al_{0.333}Zn_{0.667})_3Ti$)	*Imm*2 (44)	Al1: 2*a*, Al2: 2*b*, Zn1: 2*a*, Zn2: 2*b*, Zn3: 2*b*, Zn4: 2*b* Ti1: 2*a*, Ti2: 2*a*	−0.024468
429 ($(Al_{0.333}Zn_{0.667})_3Ti$)	*P*4/*nmm* (129)	Al1: 2*a*, Al2: 2*c*, Zn1: 2*b*, Zn2: 2*c*, Zn3: 4*f*, Ti1: 2*c*, Ti2: 2*c*	−0.033263
443 ($(Al_{0.333}Zn_{0.667})_3Ti$)	*Pmnm* (59)	Al1: 2*a*, Al2: 2*b*, Zn1: 2*a*, Zn2: 2*b*, Zn3: 2*b*, Zn4: 2*b* Ti1: 2*a*, Ti2: 2*a*	−0.032402
504 ($(Al_{0.417}Zn_{0.593})_3Ti$)	*Pmm*2 (25)	Al1: 1*b*, Al2: 1*b*, Al3: 1*c*, Al4: 1*c*, Al5: 1*d* Zn1: 1*a*, Zn2: 1*a*, Zn3: 1*b*, Zn4: 1*b*, Zn5: 1*c*, Zn6: 1*c*, Zn7: 1*d* Ti1: 1*a*, Ti2: 1*a*, Ti3: 1*d*, Ti4: 1*d*	−0.011711
583 ($(Al_{0.667}Zn_{0.333})_3Ti$)	*I*4/*mmm* (139)	Al1: 4*c*, Al2: 4*d*, Zn: 4*e*, Ti: 4*e*	−0.016714
589 ($(Al_{0.333}Zn_{0.667})_3Ti$)	*I*4/*mmm* (139)	Al1: 4*d*, Zn1: 4*c*, Zn2: 4*e*, Ti: 4*e*	−0.005477
613 ($(Al_{0.167}Zn_{0.833})_3Ti$)	$I\bar{4}m2$(119)	Al1: 2*c*, Zn1: 2*d*, Zn2: 4*e*, Zn3: 4*f*, Ti: 4*e*	−0.00000
624 ($(Al_{0.417}Zn_{0.593})_3Ti$)	$P\bar{4}m2$(115)	Al1: 1*b*, Al2: 2*e*, Al3: 2*f*, Zn1: 1*a*, Zn2: 1*c*, Zn3: 1*d*, Zn4: 2*g* Zn5: 2*g*, Ti1: 2*g*, Ti2: 2*g*	−0.017285

Note: Here, the formation energies (ΔE_f) are relative to $D0_{23}$-Al_3Ti and $D0_{23}$-Zn_3Ti.

the formation energy for the cubic $L1_2$ phase. For Zn site fractions greater than approximately 12%, the $L1_2$ phase is seen to have the lowest energy.

The pronounced effect of Zn on the stability of the $L1_2$ phase is related to the relatively strong and negative mixing energy in this phase. The mixing energy, which is defined as the difference in energy between a ternary $(Al_{1-x}Zn_x)_3Ti$ alloy and the concentration-weighted average of the energies of Al_3Ti and Zn_3Ti with the same crystal structure, is plotted in Fig. 4 for the $L1_2$ structure. In Fig. 6 the mixing energy represents the difference between the formation energies plotted by the solid lines, and the dashed lines representing ideal behavior. The mixing energy for cubic $L1_2$ is seen to be negative and relatively large in magnitude compared to the results for the tetragonal $D0_{22}$ and $D0_{23}$ compounds. Some insight into the qualitatively different mixing energies for the cubic versus the tetragonal structures can be obtained by considering the magnitudes of the effective cluster interactions plotted in Fig. 4. For each of the three structures the energetics of mixing on the Al/Zn sublattice are predicted to be dominated by pairwise interactions. For the $L1_2$ structure these ECIs are seen to be positive, favoring mixing, for all of the pairs selected by the ATAT algorithms in the generation of the sublattice-cluster-expansion. For the tetragonal $D0_{22}$ and $D0_{23}$ phases, by contrast, the pair interactions are seen to oscillate in sign, with unlike bonds favored energetically for some of the pairs and like bonds favored for others. The result of such

Table 7 Effective cluster interaction parameters (ECIs) in $L1_2$-$(Al_{1-x}Zn_x)_3Ti$, $D0_{22}$-$(Al_{1-x}Zn_x)_3Ti$, and $D0_{23}$-$(Al_{1-x}Zn_x)_3Ti$

Phase	Cluster symbol	Cluster coordinates	Cluster size, nm	Multiplicity	ECI (meV/cluster)
$L1_2$-$(Al_{1-x}Zn_x)_3Ti$	*E*(0,1)				−261.193
	E(1,1)	(0.0,0.5,0.5)		3	5.531
	E(2,1)	(0.0,0.5.0.5) (0.5,0.0,0.5)	0.28072	12	8.913
	E(2,2)	(0.5,0.5,0.0) (−0.5,0.5,0.0)	0.39700	6	4.303
	E(2,3)	(0.5,0.5,0.0) (0.5,0.5,1.0)	0.39700	3	1.403
	E(2,4)	(1.0,0.5,0.5) (0.5,−0.5,0.0)	0.48622	24	2.612
	E(2,5)	(0.5,0.5,1.0) (−0.5,0.5,0.0)	0.56144	12	0.986
	E(2,6)	(0.5,0.0,0.5) (−0.5,0.0,−0.5)	0.56144	6	3.247
	E(2,7)	(1.0,0.5,0.5) (−0.5,0.5,0.0)	0.62771	24	0.700
	E(2,8)	(0.5,0.0,0.5) (−0.5,1.0,−0.5)	0.68762	12	0.161
	E(2,9)	(1.0,0.5,0.5) (−0.5,−0.5,0.0)	0.74272	48	0.503
$D0_{22}$-$(Al_{1-x}Zn_x)_3Ti$	*E*(0,1)				160.723
	E(1,1)	(0.0,0.0,0.5)		4	62.684
	E(1,2)	(0.0,0.5,0.25)		2	−9.547
	E(2,1)	(0.0,0.5.0.25) (0.5,0.0,0.25)	0.27152	8	−9.955
	E(2,2)	(0.0,0.5,0.25) (0.5,0.5,0.0)	0.28899	16	−4.177
	E(2,3)	(0.0,0.5,0.25) (1.0,0.5,0.25)	0.38399	8	−0.581
	E(2,4)	(0.0,0.0,0.5) (0.0,1.0,0.5)	0.38399	4	5.293
	E(2,5)	(0.5,0.0,0.25) (0.5,0.0,−0.25)	0.43199	4	−2.299
	E(2,6)	(1.0,0.5,0.25) (0.5,−0.5,0.0)	0.48059	32	0.000
	E(2,7)	(0.5,0.0,0.25) (0.0,0.5,−0.25)	0.51024	16	0.333
	E(2,8)	(0.5,0.5,0.0) (0.0,0.0,0.5)	0.51024	8	−0.364
	E(2,9)	(0.0,0.5,0.25) (1.0,−0.5,0.25)	0.54304	8	0.000
	E(2,10)	(0.0,1.0,0.5) (1.0,0.0,0.5)	0.54304	4	3.891
	E(3,1)	(0.5,0.5,0.0) (0.5,0.0,0.25) (0.0,0.5,0.25)	0.28899	16	−2.886
$D0_{23}$-$(Al_{1-x}Zn_x)_3Ti$	*E*(0,1)				−234.551
	E(1,1)	(0.0,0.5,0.0)		4	−15.924
	E(1,2)	(0.0,0.5,0.25)		4	1.755
	E(1,3)	(0.0,0.0,0.375)		4	15.433
	E(2,1)	(0.0,0.5.0.25) (0.5,0.0,0.25)	0.27550	8	−7.405
	E(2,2)	(0.0,0.5,0.0) (0.5,0.0,0.0)	0.27550	8	9.757
	E(2,3)	(0.0,0.5,0.5) (0.0,0.0,0.375)	0.28506	16	8.459
	E(2,4)	(0.0,0.5,0.25) (0.5,0.5,0.125)	0.28552	16	−1.111
	E(2,5)	(0.5,0.5,0.125) (−0.5,0.5,0.125)	0.38962	8	0.000
	E(2,6)	(0.5,0.0,0.0) (−0.5,0.0,0.0)	0.38962	4	0.000
	E(2,7)	(0.0,0.5,0.25) (0.0,−0.5,0.25)	0.38962	8	0.000
	E(2,8)	(0.0,0.5,0.5) (0.0,−0.5,0.5)	0.38962	4	0.000
	E(2,9)	(0.0,0.0,0.625) (0.0,0.0,0.375)	0.41621	2	−1.443
	E(2,10)	(0.5,0.0,0.0) (0.5,0.0,0.25)	0.41685	8	7.158

Note: The empty, point, pair, and three-body clusters are labeled as *E*(0,1), *E*(1,1... *n*), *E*(2,1... *n*), and *E*(3,1 ... *n*), respectively. It may be noted that there are two and three point clusters in $D0_{22}$ and $D0_{23}$ phases, respectively, due to two (2*b*, 4*d*) and three (4*c*, 4*d*, 4*e*) Wyckoff positions for Al (or Zn) in the corresponding structure. Unlike ECIs in a binary alloy system, the pair and three-body interaction parameters in a pseudobinary system should be considered as pseudo-pair and pseudo-three-body interaction parameters due to the interactions with the spectator specie. Coordinates are in fraction of lattice vectors (the *z* coordinates for the $D0_{23}$ lattice are rounded to the nearest 1/8, for clarity). Cluster size is defined as the length of the longest pair contained in the cluster (calculated using the lattice parameters of Al_3Ti in the corresponding structure)

frustrated ordering behavior is a near cancellation of bonding and clustering terms in the energy, leading to nearly ideal mixing behavior for Al and Zn in these tetragonal structures. Further analysis related to the stabilizing effect of Zn on the $L1_2$ structure relative to $D0_{22}$ and $D0_{23}$ will be presented in the next subsection in terms of calculated electronic densities of states.

It is interesting to consider further the relatively good agreement displayed between cluster-expansion and supercell results in Fig. 6. Specifically, the SC method makes use of particular ordered configurations to model the composition dependence of the formation energy, while the SCE results plotted in Fig. 6 correspond to random configurations. Good agreement between the two results implies that

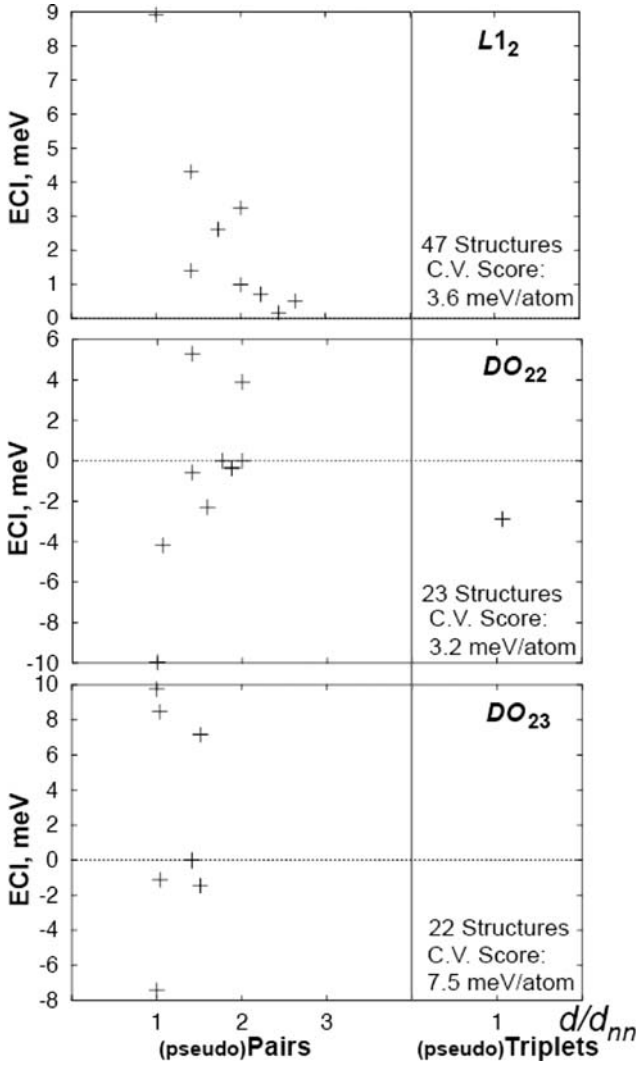

Fig. 4 Calculated ECIs versus cluster diameter (normalized by nearest neighbor distance) in $L1_2$-, $D0_{22}$-, and $D0_{23}$-$(Al,Zn)_3Ti$

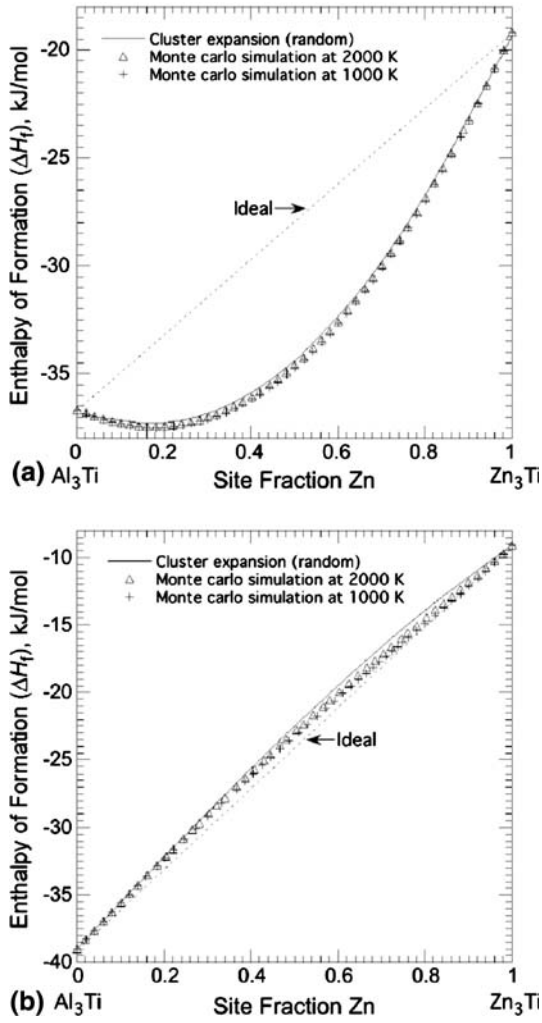

Fig. 5 Comparison of calculated heats of formation by cluster expansion and Monte-Carlo simulation of (a) $L1_2$, and (b) $D0_{22}$ phases along the pseudobinary section Al_3Ti-Zn_3Ti. These demonstrate that the effect of short-range-order on the heat of formation is negligible as compared to that predicted by the cluster expansion for random mixing. The reference states are fcc-Al, cph-Ti and cph-Zn

the difference in energy between ordered and random configurations are relatively small in this system. This interpretation is supported by the results of SCE-based Monte-Carlo simulations performed as a function of temperature for the $L1_2$ and $D0_{22}$ phases plotted in Fig. 5. In systems where ordering tendencies are more pronounced, the good level of agreement between SC and SCE methods found here may not be generally expected, and the SCE approach, while computationally more demanding, is generally preferred as it provides a framework for incorporating configurational effects in calculations of alloy formation energies.

3.5 Electronic Density of States Along Al_3Ti-Zn_3Ti

Further insight into the origin of the stabilizing effect of Zn upon the stability of the cubic $L1_2$ relative to the tetragonal $D0_{22}$ and $D0_{23}$ structures can be gained by considering the calculated electronic densities of states shown in Fig. 7. We start with the results for Al_3Ti shown in Fig. 7(a). For each structure the total DOS are characterized by a pronounced dip near the Fermi level. This so-called pseudo-gap feature[27] has been extensively discussed in the literature as reflecting a separation between bonding and anti-bonding states associated with hybridization between the Al p and Ti d electrons. At the Al_3Ti composition the $L1_2$ structure has its Fermi level lying to the right (i.e., at higher energies) relative to the pseudo-gap minimum, while for the tetragonal structures the Fermi levels are within or just to the left (lower energies) of the pseudo-gap. These results suggest that the stability of the tetragonal structures relative to cubic $L1_2$ can be interpreted as a reflection of the increased occupation of anti-bonding states in the latter.[27] Based on this interpretation, a rigid-band model would predict that substitution of Al by Zn should increase the

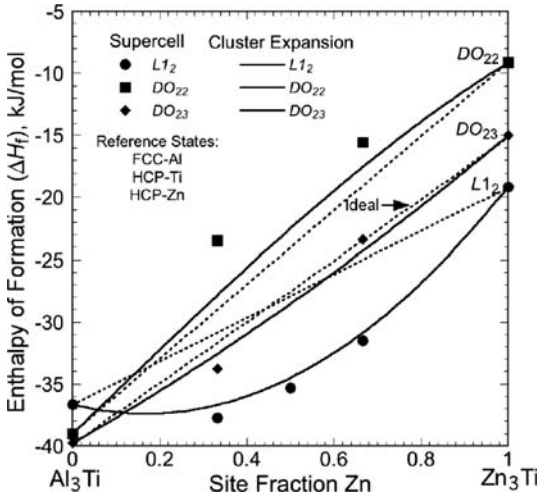

Fig. 6 Calculated heats of formation of $L1_2$, $D0_{22}$, and $D0_{23}$ phases along the pseudobinary section Al_3Ti-Zn_3Ti. The reference states are fcc-Al, hcp-Ti, and hcp-Zn. The supercell results are shown to be reasonably good with those predicted by the cluster expansion for random mixing.

stability of $L1_2$ relative to $D0_{22}$ and $D0_{23}$ phases since Zn has one less valence electron than Al, and alloying with this element should have the effect of moving the Fermi level to lower energies relative to the pseudo-gap minima.

The results in Fig. 7(b), obtained for supercells with composition $(Al_{0.667}Zn_{0.333})_3Ti$, are in qualitative agreement with this band-filling picture. The Fermi level for the $L1_2$ structure is seen to lie within the pseudo-gap minimum, corresponding to near optimal filling of the bonding states. By contrast the Fermi level has moved to the left, leading to lower occupations of the bonding states, for the tetragonal structures. The stabilization of the $L1_2$ structure and destabilization of the tetragonal structures induced by substituting Zn for Al are thus entirely consistent with a band-filling picture where the reduction of electron per atom ratio leads to optimum filling of bonding states in the cubic phase (increasing cohesion) and decreased occupation of these states in $D0_{22}$ and $D0_{23}$ (leading to decreased cohesion).

The results in Fig. 7(c), for the composition $(Al_{0.333}Zn_{0.667})_3Ti$ where Fig. 6 shows a maximum energy difference between $L1_2$ and the higher-energy tetragonal structures, remain qualitatively consistent with the band-

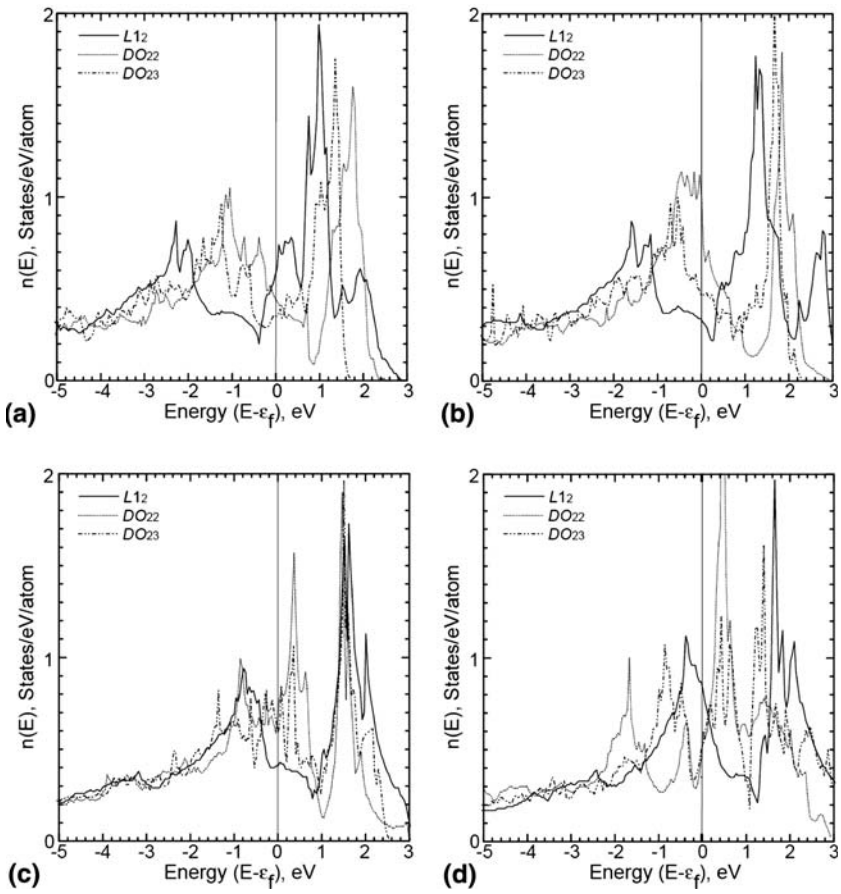

Fig. 7 A comparison of total electronic density of states in $L1_2$, $D0_{22}$, and $D0_{23}$ along the pseudobinary section Al_3Ti-Zn_3Ti: (a) Al_3Ti, (b) $(Al_{0.667}Zn_{0.333})_3Ti$, (c) $(Al_{0.333}Zn_{0.667})_3Ti$, and (d) Zn_3Ti

filling picture described in the previous two paragraphs. The results in Fig. 7(d), however, show qualitative differences in the shapes of the DOS, particularly for the tetragonal structures, indicating the limitations of the rigid-band model applied over the entire composition range.

4. Conclusions

The thermodynamic and mechanical stabilities of the $L1_2$, $D0_{22}$, and $D0_{23}$ structures along the pseudobinary section Al_3Ti-Zn_3Ti were investigated via first-principles methods. The relative thermodynamic stability of the structures considered was investigated by both supercell and cluster expansion methods. Due to the relatively small energy differences between ordered and disordered states (on the Al, Zn sublattice) in this system, the supercell and cluster expansion methods give very similar results. As a consequence of this result, the Bragg-Williams approximation is expected to be reliable in this system and agrees with more accurate Monte-Carlo simulations that account for the possible presence of short-range order.

While the thermodynamically stable structure of Al_3Ti is $D0_{23}$, the substitution of Zn on the Al sublattice of Al_3Ti is found to stabilize the $L1_2$ structure relative to the $D0_{22}$ and $D0_{23}$ structures. These trends can be intuitively understood in terms of a simple rigid-band picture in which the addition of Zn reduces the effective number of valence electrons. The Fermi level in $D0_{22}$ and $D0_{23}$ Al_3Ti lies in a pseudo-gap, which is indicative of increased stability. In contrast, the Fermi level lies in the anti-bonding states in the $L1_2$ structure. The addition of Zn lowers the Fermi level, moving it towards optimal filling of the bonding states in the $L1_2$ structure but away from optimal filling in the case of the $D0_{22}$ and $D0_{23}$ structures, thus stabilizing the $L1_2$ structure relative to the other two.

Our results thus indicate that Zn substitution in Al_3Ti alloys represents a promising way to achieve the stabilization of $L1_2$ precipitates in order to favor the formation of a microstructure associated with desirable mechanical properties.

The calculated zero-temperature elastic constants show that the binary end members are mechanically stable in all three ordered structures, suggesting that the compounds and solid solutions considered in this study are experimentally accessible.

Acknowledgments

This research was supported by the US Department of Energy, Office of Basic Energy Sciences, under Contract Nos. DE-FG02-02ER45997 (GG) and DOE-FG02-01ER45910 (AvdW and MA). Supercomputing resources were provided by the National Partnership on Advanced Computational Infrastructure (NPACI) at the University of Michigan at Ann Arbor and at the University of Illinois at Urbana-Champaign.

References

1. M.Y. Drits, L.B. Ber, Y.G. Bykov, L.S. Toropova, and G.K. Anastasyeva, Aging of Al-0.3 at.% Sc Alloy, *Fiz. Met. Metallov.*, 1984, **57**, p 1172-1179
2. D.N. Seidman, E.A. Marquis, and D.C. Dunand, Precipitation Strengthening at Ambient and Elevated Temperatures of Heat-treatable Al(Sc) Alloys, *Acta Mater.*, 2002, **50**, p 4021-4035
3. M.S. Zedalis and M.E. Fine, Precipitation and Ostwald Ripening in Dilute Al Base-Zr-V Alloys, *Metall. Trans. A*, 1986, **17A**, p 2187-2198
4. V.R. Parameswaran, J.R. Weertman, and M.E. Fine, Coarsening Behavior of $L1_2$ Phase in an Al-Zr-Ti Alloy, *Scripta Met.*, 1989, **23**, p 147-150
5. S. Fujikawa, Solid-State Diffusion in Light Metals, *J. Jpn. Inst. Light Metals*, 1996, **46**, p 202-215
6. Y. Nakayama and H. Mabuchi, Formation of Ternary $L1_2$ Compounds in Al_3Ti-Base Alloys, *Intermetallics*, 1993, **1**, p 41-48
7. A. Raman and K. Schubert, Uber den Aufbau Einiger zu $TiAl_3$ Verwandter Legierungsreihen. I. Untersuchungen in Einigen T^4-Zn-Al-, T^4-Zn-Ga- und T^4-Ga-Ge-Systemen, *Z. Metallkde.*, 1965, **56**, p 40-43
8. G. Kresse and J. Furthmüller, Efficient Iterative Schemes of Ab Initio Total-energy Calculations Using a Plane-wave Basis Set, *Phys. Rev. B*, 1996, **54**, p 11169-11186
9. G. Kresse and J. Furthmüller, Efficiency of Ab-Initio Total Energy Calculations for Metals and Semi-conductors Using a Plane-wave Basis Set, *Comput. Mater. Sci.*, 1996, **6**, p 15-50
10. D. Vanderbilt, Soft Self-consistent Pseudo Potential in a Generalized Eigenvalue Formalism, *Phys. Rev. B*, 1990, **41**, p 7892-7895
11. J.P. Perdew and Y. Wang, Accurate and Simple Analytic Representation of the Electron-Gas Correlation-Energy, *Phys. Rev. B*, 1992, **45**, p 13244-13249
12. G. Ghosh and M. Asta, First-Principles Calculations of Structural Energetics of Al-TM(TM = Ti,Zr,Hf) Intermetallics, *Acta Mater.*, 2005, **53**, p 3225-3252
13. A. van de Walle and G. Ceder, Automating First-Principles Phase Diagram Calculations, *J. Phase Equilibria*, 2002, **23**, p 348-359
14. A. van de Walle, M. Asta, and G. Ceder, The Alloy Theoretic Automated Toolkit: A User Guide, *CALPHAD J.*, 2002, **26**, p 539-553
15. A. van de Walle and M. Asta, Self-Driven Lattice-Model Monte Carlo Simulations of Alloy Thermodynamic Properties and Phase Diagrams, *Model. Simul. Mater. Sci. Eng.*, 2002, **10**, p 521-538
16. P.D. Tepesch, G.D. Garbulsky, and G. Ceder, Model for Configurational Thermodynamics in Ionic Systems, *Phys. Rev. Lett.*, 1995, **74**, p 2272-2275
17. G. Ceder, A. van der Ven, C. Marianetti, and D. Morgan, First-Principles Alloy Theory in Oxides, *Model. Simul. Mater. Sci. Eng.*, 2000, **8**, p 311-321
18. J.M. Sanchez, F. Ducastelle, and D. Gratias, Generalized Cluster Description of Multicomponent Systems, *Physica*, 1984, **128**, p 334-350
19. P. Vinet, J.H. Rose, J. Ferrante, and J.R. Smith, Universal Feature of the Equation of State in Solids, *J. Phys.: Condens. Matter.*, 1989, **1**, p 1941-1963
20. G.P. Vassilev, X.J. Liu, and K. Ishida, Reaction Kinetics and Phase Diagram Studies in the Ti-Zn System, *J. Alloys Compd.*, 2004, **375**, p 162-170

21. G. Ghosh, S. Delsante, G. Borzone, M. Asta, and R. Ferro, Phase Stability and Cohesive Properties of Ti-Zn Intermetallics: First-Principles Calculations and Experimental Results, *Acta Mater.*, 2006, **54**, p 4977-4997
22. M.J. Mehl, B.M. Klein, and A. Papaconstatopolous, First-Principles Calculations of Elastic Properties, *Intermetallic Compounds: Principles*, J.H. Westbrook and R.L. Fleischer, Eds. Vol. 1, Wiley, New York, 1994, p 195-210
23. C.L. Fu, Electronic, Elastic, and Fracture Properties of Trialuminides Alloys—Al_3Sc and Al_3Ti, *J. Mater. Res.*, 1990, **5**, p 971-979
24. M.H. Yoo and C.L. Fu, Fundamental-Aspects of Deformation and Fracture in High-Temperature Ordered Intermetallics, *ISIJ Int.*, 1991, **31**, p 1049-1062
25. M. Nakamura and K. Kimura, Elastic-Constants of $TiAl_3$ and $ZrAl_3$ Single-Crystals, *J. Mater. Sci.*, 1991, **26**, p 2208-2214
26. D.C. Wallace, *Thermodynamics of Crystals*. Wiley, New York, 1972
27. A.E. Carlsson and P.J. Meschter, Ab Initio Calculations, *Intermetallic Compounds: Principles*, J.H. Westbrook and R.L. Fleischer, Eds. Vol. 1, Wiley, New York, 1994, p 55-76